Journal of Sound and Vibration (2002) **254**(3), 575–593
doi:10.1006/jsvi.2001.4136, available online at http://www.idealibrary.com on IDEAL®

APPROXIMATING THE HYSTERETIC DAMPING MATRIX BY A VISCOUS MATRIX FOR MODELLING IN THE TIME DOMAIN

D. J. HENWOOD

School of Computing and Mathematical Sciences, University of Brighton, Lewes Road, Moulsecoomb, Brighton BN2 4GJ, England

(*Received* 28 *February* 2001, *and in final form* 3 *October* 2001)

The paper is concerned with modelling the dynamic behaviour of a structure with damping. Hysteretic damping is commonly accepted to be reasonably accurate in some circumstances, but can only be applied directly in the frequency domain. Dynamic (time) behaviour, however, is most conveniently predicted by a viscous model. A damping matrix is constructed for use in the viscous equation which gives a dissipation of energy approximating to the hysteretic model. The approximation is justified by comparing results in the frequency and time domains and against measured data from a loudspeaker diaphragm. The ability of the matrix to reflect different damping in various components of the structure is considered, together with predicted natural frequencies and modes.

1. INTRODUCTION

1.1. BACKGROUND

Material damping, the loss of energy occurring through motion in a structure, comes from many causes even when only a single material is involved, and its accurate mathematical representation is difficult [1–3].

If the damping in a system has its origin in linear viscoelastic effects within the material (as opposed to locally non-linear effects associated with structural junctions) then the effects can be exactly characterized via complex moduli. This follows from the "viscoelastic principle" see references [4, 5]. The complex moduli are defined in the frequency domain, and because of the well-known causality problem [6], they cannot be constant. However, as an empirical fact of observation, for moderate audio frequencies these moduli often turn out to be rather slowly varying in frequency, so that the "hysteretic model" is often used as a convenient approximation (provided it is used with care).

The origin of the hysteretic assumption does not come from matching the forms of transfer functions, but from measuring modal damping factors and observing the constant-Q behaviour. This means that the most natural thing to match, if trying to approximate the behaviour within a viscous model, is not so much particular values of the transfer function as the complex poles and residues of the transfer function. For the simplest case in which the mass matrix of a system is a multiple of the unit matrix, one way to achieve constant-Q-behaviour is by using a damping matrix which is the symmetric square root of the stiffness matrix. This fact, although not emphasized, appears in the famous paper by Caughey [7]. However, this is unlikely to be helpful for complicated structures.

0022-460X/02/$35.00

If damping is small, then modal damping factors can be calculated by post-processing elastic modes and frequencies, using Rayleigh's principle. This approach can allow for spatial variations, and for frequency varying complex moduli [8, 9]. In this paper, a method for approximating to hysteretic damping is proposed which does not, in itself, require damping to be small, although its accuracy may decline as damping grows. An example is treated in detail which uses a relatively large loss factor. The outcome is mainly considered qualitatively, as a general theory for accuracy has not been developed.

The situation addressed here is of a structure made up of different materials and for which the hysteretic model is considered acceptable with damping information available in the form of material loss factors. The interest is in the transient response of the structure to a time excitation which is not periodic. The problem can be solved in the frequency domain and the solution be transferred to the time domain according to the correspondence principle [5]. However, there is the theoretical difficulty with causality and in practice the use of the inverse fast Fourier transform calls for considerable care to be accurate, see reference [10, chapter 12]. It is more straightforward to work directly in the time domain, and there is an established method, see reference [11, chapter 8], which solves the equations if the damping is included through a viscous rather than a hysteretic matrix. Thus, as a mathematical convenience, it would be helpful to have a method for deriving a viscous matrix from the matrix of the hysteretic model containing the localized damping information. This paper describes such a method.

1.1.1. *A statement of the problem to be considered*

It is assumed that

$$\mathbf{M}\ddot{\mathbf{u}}(t) + (\mathbf{K} + \mathrm{i}\mathbf{H})\mathbf{u}(t) = \mathbf{g}(t), \tag{1}$$

provides an acceptable model in the frequency domain, where $\mathbf{u}(t)$ contains the N structure degrees of freedom, and $\mathbf{M}$ and $\mathbf{K}$ are the standard mass and stiffness matrices (formed by the finite element method in our case). Damping is incorporated through modifying the modulus of elasticity, E, by adding a term with a $\pi/2$ phase shift,

$$E(1 + \mathrm{i}\eta), \quad \mathrm{i} = \sqrt{-1}.$$

The (assumed) constant η is called the damping *loss factor* and physically measures the proportion of energy lost in a cycle. Thus for a structure made from a single material damping enters the equation of motion through the term

$$\mathbf{K}(1 + \mathrm{i}\eta)\mathbf{u}(t).$$

If a structure is made up of several different materials the form becomes

$$\mathbf{K}(1 + \mathrm{i}\mathbf{H})\mathbf{u}(t),$$

where the matrix $\mathbf{H}$ reflects the distribution of the damping.

To obtain a time response it is convenient to work with the viscous damping model

$$\mathbf{M}\ddot{\mathbf{u}}(t) + \mathbf{C}\dot{\mathbf{u}}(t) + \mathbf{K}\mathbf{u}(t) = \mathbf{g}(t). \tag{2}$$

For the type of problem considered here there is no clear indication of how to form **C**. For Rayleigh (proportional) damping, $\mathbf{C} = \alpha\mathbf{M} + \beta\mathbf{K}$. The mathematics is simplified, but in general there will not be suitable parameters α, β to represent a structure. The concern of this paper is to devise a suitable **C** to approximate to hysteretic damping, equation (1). Approximating one form by the other has been addressed for a one-degree-of-freedom system in reference [3]. Here the subject is revisited and extended to a general structure.

2. CONSTRUCTING AN EQUIVALENT VISCOUS DAMPING MATRIX

2.1. ONE DEGREE OF FREEDOM

A one-degree-of-freedom system is initially examined in order to establish a method that can then be extended to the (finite element) model of a more general structure. Consider the hysteretic damping model which is to be transformed to the frequency domain,

$$m\ddot{u}(t) + k(1 + \mathrm{i}\eta)u(t) = g(t), \tag{3}$$

where m is the mass, k the stiffness, η the loss factor or hysteretic damping factor and g is the forcing function. For sinusoidal forcing,

$$g(t) = g\mathrm{e}^{\mathrm{i}\omega t}, \quad u(t) = u_h\mathrm{e}^{\mathrm{i}\omega t} \tag{4}$$

and factoring out the time term,

$$-m(\omega)^2 u_h + k(1 + \mathrm{i}\eta)u_h = g. \tag{5}$$

Introducing the natural frequency of the undamped system

$$\omega_n = \sqrt{\frac{k}{m}},$$

equation (5) becomes

$$(-\omega^2 + \mathrm{i}\eta\omega_n^2 + \omega_n^2)u_h = \frac{g}{m}. \tag{6}$$

The corresponding viscous damping model is

$$m\ddot{u}(t) + c\dot{u}(t) + ku(t) = g(t), \tag{7}$$

where c is the damping coefficient. The sinusoidal response is similarly given by

$$\left(-\omega^2 + \mathrm{i}\frac{c}{m}\omega + \omega_n^2\right)u_v = \frac{g}{m}. \tag{8}$$

Clearly, as ω varies, the two equations (6) and (8) cannot give the same values to the two frequency domain solutions u_h and u_v. Suppose the roots of the homogeneous forms of the equations (which correspond to the poles of the transfer function) are compared. They are for the viscous and hysteretic models, in the first quadrant of the complex plane,

$$z_h = \omega_n(1 + \mathrm{i}\eta)^{1/2} \quad \text{and} \quad z_v = \sqrt{\omega_n^2 - \left(\frac{c}{2m}\right)^2} + \mathrm{i}\frac{c}{2m}.$$

Ideally, c would be chosen so that these are the same point as η varies, but simple manipulation shows that this is not possible. The best that can be achieved is that a measure of the distance between them is minimized. Consider an obvious choice for the measure

$$\frac{\mathrm{d}}{\mathrm{d}c}|z_h - z_v|^2 = 0,$$

$$\frac{\mathrm{d}}{\mathrm{d}c}\left|\omega_n(1+\mathrm{i}\eta)^{1/2} - \sqrt{\omega_n^2 - \left(\frac{c}{2m}\right)^2} - \mathrm{i}\frac{c}{2m}\right|^2 = 0.$$

Setting $\varepsilon = \arctan(\eta)$

$$\frac{\mathrm{d}}{\mathrm{d}c}\left\{\left[\omega_n(1+\mathrm{i}\eta)^{1/4}\cos\left(\frac{\varepsilon}{2}\right) - \sqrt{\omega_n^2 - \left(\frac{c}{2m}\right)^2}\right]^2 + \left[\omega_n(1+\mathrm{i}\eta)^{1/4}\sin\left(\frac{\varepsilon}{2}\right) - \left(\frac{c}{2m}\right)\right]^2\right\} = 0.$$

This leads eventually to

$$c = 2m\omega_n \sin\left[\frac{(\arctan\eta)}{2}\right] \tag{9}$$

$$\text{or, if } \eta \ll 1 \qquad c \approx m\omega_n\eta. \tag{10}$$

Neither of these values for c, equations (9) and (10) will give exact correspondence over a frequency range, but rather an approximation according to the chosen criterion. Figure 1 shows how $\sin[(\arctan\eta)/2]$ and η differ; there is very close agreement up to $\eta = 0{\cdot}4$ and it remains good up to about $\eta = 1$.

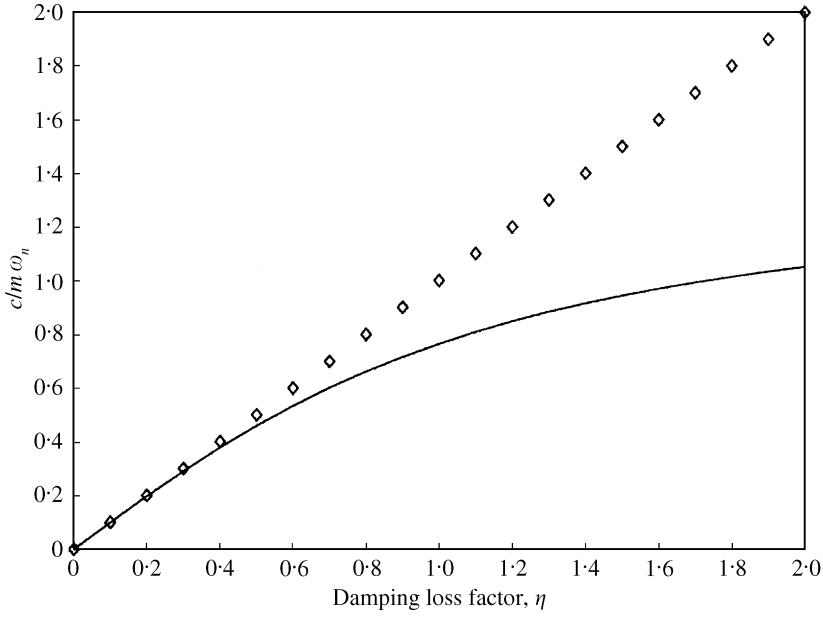

Figure 1. To compare a near-optimal choice for $c/(m\omega_n)$, i.e., η shown by (◇), with an optimal solution for $c/(m\omega_n)$, i.e., $2\sin[(\arctan\eta)/2]$, shown by (——).

If approximation (10) is substituted into equation (8) and the result compared with equation (6), the choice for c can be interpreted as that which makes the two equations identical when ω is at the modal frequency ω_n. This way of choosing c carries over straightforwardly from a single equation to a system representing a complex structure, and has been used for the work of the paper. A further justification is that, as shown later, it does seem to work reasonably well. The alternative (and there must be others) of equation (9) appears not to be so easy to apply to a general structure and has not been explored by the author.

Note for later reference: an estimate needs to be made of a *modal loss factor* in section 4.2 where the modal decay rates and frequencies are available. To do this, equation (10) may be rearranged,

$$\eta = \frac{c}{m}\frac{1}{\omega_n} = 2\left(\frac{c}{2m}\right)\left(\frac{1}{\omega_n}\right) = 2\,\frac{\text{decay rate}}{\text{natural frequency}}. \tag{11}$$

So the right-hand side of equation (11) may be used for an estimate, which may then be compared with material loss factors.

Adopting the choice for c given in equation (10), the two damping models are now compared. For hysteretic, the damped natural frequency, ω_h, is given by

$$-\omega_h^2 + (\mathrm{i}\eta + 1)\omega_n^2 = 0,$$

$$\text{i.e., } \frac{\omega_h}{\omega_n} = (1 + \mathrm{i}\eta)^{1/2}$$

$$= \left(1 + \frac{\eta^2}{8} + \cdots\right) + \mathrm{i}\left(\frac{\eta}{2} - \frac{\eta^3}{16} + \cdots\right), \text{ assuming } \eta < 1$$

$$= \delta_h + \mathrm{i}\gamma_h \text{ say.}$$

Since $\mathrm{e}^{\mathrm{i}\omega_h t} = \mathrm{e}^{\mathrm{i}\omega_n(\delta_h + \mathrm{i}\gamma_h)t} = \mathrm{e}^{-\gamma_h\omega_n t}\mathrm{e}^{\mathrm{i}\delta_h\omega_n t}$, then δ_h and γ_h are factors in the frequency and decay rate

$$\delta_h\omega_n \approx \left(1 + \frac{\eta^2}{8}\right)\omega_n, \quad \gamma_h\omega_n \approx \frac{\eta}{2}\omega_n.$$

The corresponding viscous damping model has a natural frequency given by

$$-\omega_v^2 + \mathrm{i}\eta\omega_v\omega_n + \omega_n^2 = 0,$$

$$\text{i.e., } \frac{\omega_v}{\omega_n} = \mathrm{i}\,\frac{\eta}{2} \pm \sqrt{1 - \frac{\eta^2}{4}}$$

$$= \delta_v + \mathrm{i}\gamma_v \text{ considering only the positive frequency.}$$

Thus, as for hysteretic damping δ_v and γ_v are factors in the frequency and decay rate

$$\delta_v\omega_n \approx \left(1 - \frac{\eta^2}{8}\right)\omega_n, \quad \gamma_v\omega_n = \frac{\eta}{2}\omega_n.$$

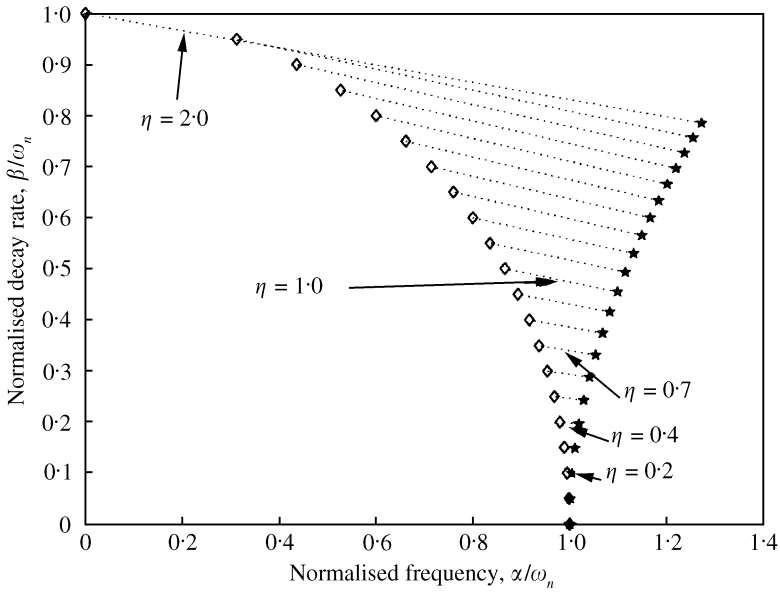

Figure 2. To show the influence of the loss factor on the decay rates and normalized frequency of the hysteretic (∗) and equivalent viscous (◇) damping models, for a single-degree-of-freedom system.

A comparison of the normalized frequency and decay rates from the two models is shown in Figure 2.

Notes on the comparison between the models

- For small η the two models are similar: for example if $\eta < 0{\cdot}5$, the two normalized frequency and decay rates differ by less than 6 and 3%, respectively, of the hysteretic value.
- Since $\gamma_v > \gamma_h$, a slightly higher decay rate is predicted by the viscous damping model, and the difference increases with increasing η.
- Since $\delta_v < 1 < \delta_h$, the viscous model indicates that the effect of damping is to reduce natural frequency and the hysteretic to raise it. The former corresponds to the generally expected behaviour, rather than the latter [3].
- For the equivalent viscous equation critical damping occurs when $\eta = 2$.
- The acausal nature of the hysteretic scheme, see reference [3, 6], means that the two damping models can never be made identical. The poles can only be matched approximately, and not uniquely as there are different ways of quantifying the difference between the poles. The approach adopted can be understood as making the two equations the same at the natural frequency. The decay rate predicted by the equivalent viscous model is higher and becomes progressively more so as η increases.

2.2. MODELLING A GENERAL STRUCTURE

Consider the general case: in the frequency domain the two equations (2), (1) are

$$[-\mathbf{M}\omega^2 + \mathrm{i}\omega\mathbf{C} + \mathbf{K}]\mathbf{u}_v = \mathbf{g} \tag{12}$$

and

$$[-\mathbf{M}\omega^2 + \mathrm{i}\mathbf{H} + \mathbf{K}]\mathbf{u}_h = \mathbf{g}, \tag{13}$$

where $\mathbf{u}_v$, $\mathbf{u}_h$ are the frequency domain displacement vectors derived from the viscous and hysteretic damping models and $\mathbf{g}$ is a vector giving the spatial distribution of the force. Suppose that $\mathbf{X}$, $\mathbf{D}$ form the eigensystem of $\mathbf{M}$ and $\mathbf{K}$ so that

$$\mathbf{KX} = \mathbf{MXD},$$

where the columns of $\mathbf{X}$ are the eigenvectors (modes) and the diagonal matrix $\mathbf{D}$ contains the natural frequencies:

$$\mathbf{D} = \mathrm{diag}\{\omega_1^2, \omega_2^2, \ldots, \omega_N^2\}.$$

Applying the eigenmatrices to partially uncouple equation (13) gives

$$\mathbf{MX}[-\mathbf{I}(\omega)^2 + \mathrm{i}(\mathbf{MX})^{-1}\mathbf{HX} + \mathbf{D}](\mathbf{X}^{-1}\mathbf{u}_h) = \mathbf{g}$$

$$\text{or } [-\mathbf{I}(\omega)^2 + \mathrm{i}\mathbf{B}^{-1}\mathbf{HX} + \mathbf{D}]\mathbf{w}_h = \mathbf{k}, \tag{14}$$

where

$$\mathbf{B} = \mathbf{MX}, \quad \mathbf{w}_h = \mathbf{X}^{-1}\mathbf{u}_h, \quad \mathbf{k} = \mathbf{B}^{-1}\mathbf{g}.$$

The corresponding equation for viscous damping, equation (12), is

$$[-\mathbf{I}\omega^2 + \mathrm{i}\omega\mathbf{B}^{-1}\mathbf{CX} + \mathbf{D}]\mathbf{w}_v = \mathbf{k}. \tag{15}$$

Consider first the simple case where $\mathbf{H} = \eta\mathbf{K}$ and system (14) uncouples to

$$[-\mathbf{I}\omega^2 + \mathrm{i}\eta\mathbf{D} + \mathbf{D}]\mathbf{w}_h = \mathbf{k}. \tag{16}$$

The set of equations (15) cannot be made the same as equation (16) for all ω but it is possible to make pairs of corresponding equations to be the same at one frequency (different for each pair). So following the method used in the previous section, 2.1, which was derived from approximately matching poles, we choose to equate the pairs at the corresponding natural frequency, i.e., where ω takes the sequence of values

$$\{\omega_1, \omega_2, \ldots, \omega_N\}.$$

This set of values is the diagonal of the matrix $\mathbf{D}^{1/2}$.

Thus, we choose $\mathbf{C}$ so that

$$\mathbf{D}^{1/2}\mathbf{B}^{-1}\mathbf{CX} = \eta\mathbf{D}$$

$$\text{or} \quad \mathbf{C} = \eta\mathbf{MXD}^{1/2}\mathbf{X}^{-1}.$$

More generally when $\mathbf{H}$ will not allow uncoupling, i.e., is not a linear combination of $\mathbf{M}$ and $\mathbf{K}$, it is still possible to make the corresponding pairs of equations (15) and (16) the same at the natural frequencies. Here, and in the previous simpler case, it does not mean that the

solution is exact at the natural frequencies, only that the individual rows of the corresponding matrices are the same at these particular frequencies.

If the matrix $\mathbf{B}^{-1}\mathbf{HX}$ is not diagonal and the system is still coupled, row j is

$$[-\omega^2 + \omega_j^2](\mathbf{w}_h)_j + \mathrm{i}\sum_{c=1}^{N}(\mathbf{B}^{-1}\mathbf{HX})_{jc}(\mathbf{w}_h)_c = k_j, \quad j = 1, 2 \ldots N.$$

Similarly, the viscous frequency domain displacement can be expressed for row j as

$$[-\omega^2 + \omega_j^2](\mathbf{w}_v)_j + \mathrm{i}\omega\sum_{c=1}^{N}(\mathbf{B}^{-1}\mathbf{CX})_{jc}(\mathbf{w}_v)_c = k_j, \quad j = 1, 2 \ldots N. \tag{17}$$

Setting ω_j for ω in the summation term and combining the row equations (17) gives

$$[-\mathbf{I}\omega^2 + \mathrm{i}\mathbf{D}^{1/2}\mathbf{B}^{-1}\mathbf{CX} + \mathbf{D}]\mathbf{w}_v = \mathbf{k}.$$

Thus, we choose $\mathbf{C}$ so that

$$\mathbf{D}^{1/2}\mathbf{B}^{-1}\mathbf{CX} = \mathbf{B}^{-1}\mathbf{HX},$$

$$\mathbf{C} = \mathbf{B}\mathbf{D}^{-1/2}\mathbf{B}^{-1}\mathbf{H} \tag{18}$$

$$\text{alternatively, } \mathbf{C} = \mathbf{X}^{-\mathrm{T}}\mathbf{D}^{-1/2}\mathbf{X}^{\mathrm{T}}\mathbf{H}, \tag{19}$$

the last expression following from diagonalizing $\mathbf{M}$ by $\mathbf{X}$, i.e.,

$$\mathbf{X}^{\mathrm{T}}\mathbf{MX} = \mathrm{diag}\{m_1\, m_2 \ldots\} = \mathbf{D}_m \text{ say,}$$

$$\text{so that } \mathbf{B}\mathbf{D}^{-1/2}\mathbf{B}^{-1}\mathbf{H} = \mathbf{X}^{-\mathrm{T}}\mathbf{D}_m\mathbf{D}^{-1/2}\mathbf{D}_m^{-1}\mathbf{X}^{\mathrm{T}}\mathbf{H} = \mathbf{X}^{-\mathrm{T}}\mathbf{D}^{-1/2}\mathbf{X}^{\mathrm{T}}\mathbf{H}.$$

3. SOLUTION IN THE TIME DOMAIN

Having obtained a matrix $\mathbf{C}$ which approximates to hysteretic damping we now consider producing the time solution of equation (2)

$$\mathbf{M}\ddot{\mathbf{u}}(t) + \mathbf{C}\dot{\mathbf{u}}(t) + \mathbf{K}\mathbf{u}(t) = \mathbf{g}(t).$$

3.1. A NOTE ON THE LAPLACE METHOD

For a general driving function $\mathbf{g}$ a numerical time-stepping procedure such as the Newmark-beta method is necessary. A general discussion of step by step methods is given in reference [12]. However, if $\mathbf{g}$ can be expressed in terms of elementary functions, then the Laplace method will provide an analytic time solution thus avoiding any concern with stability or numerical errors beyond those due to rounding. Details are given in [11, chapter 8]. The types of driving function used in the examples are an impulse, a raised cosine form of impulse (at frequency $\omega_0/(2\pi)$) and a tone burst of n cycles; they all are

suitable for the Laplace transform;

$$\delta(t),$$

$$(1 - \cos(\omega_0 t))\left[\mathrm{H}(t) - \mathrm{H}\left(t - \frac{2\pi}{\omega_0}\right)\right],$$

$$\sin(\omega_0 t)\left[\mathrm{H}(t) - \mathrm{H}\left(t - \frac{2\pi n}{\omega_0}\right)\right],$$

where $\mathrm{H}(t-\tau)$ is the unit step function

$$\mathrm{H}(t-\tau) = \begin{cases} 0, & t < \tau, \\ 1, & t > \tau. \end{cases}$$

3.2. A NOTE ON COMPUTING ENERGY

Information on the flow of energy in a structure is also available and as it will be used later, an outline of the computation is given here.
Multiply equation (2) by $\dot{\mathbf{u}}^{\mathrm{T}}(t)$

$$\dot{\mathbf{u}}^{\mathrm{T}}(t)\mathbf{M}\ddot{\mathbf{u}}(t) + \dot{\mathbf{u}}^{\mathrm{T}}(t)\mathbf{C}\dot{\mathbf{u}}(t) + \dot{\mathbf{u}}^{\mathrm{T}}(t)\mathbf{K}\mathbf{u}(t) = \dot{\mathbf{u}}^{\mathrm{T}}(t)\mathbf{g}(t),$$

and integrate on $[0, t]$ to give

$$\tfrac{1}{2}\dot{\mathbf{u}}^{\mathrm{T}}(t)\mathbf{M}\dot{\mathbf{u}}(t) + \int_0^t \dot{\mathbf{u}}^{\mathrm{T}}(\tau)\mathbf{C}\dot{\mathbf{u}}(\tau)\,\mathrm{d}\tau + \tfrac{1}{2}\mathbf{u}^{\mathrm{T}}(t)\mathbf{K}\mathbf{u}(t) = \int_0^t \dot{\mathbf{u}}^{\mathrm{T}}(\tau)\mathbf{g}(\tau)\,\mathrm{d}\tau.$$

The first term is the structural kinetic energy and the third is the potential (strain) energy. The second term is the energy dissipated due to damping and the right-hand side of the equation is the work done by the external force.

It follows from the construction of the finite element global matrices

$$\mathbf{M} = \sum_{e=1}^{E} \mathbf{M}^e \quad \text{and} \quad \mathbf{K} = \sum_{e=1}^{E} \mathbf{K}^e,$$

where E is the number of elements forming the structure, that energy information can also be obtained at the element level.

The eigenvalues and eigenvectors from which the solution is constructed are complex. However, the original equation (2) is real and the initial conditions are real, so the solution must be real. In forming the solution the imaginary parts of the complex numbers should cancel, but numerical computation will, most probably, introduce small errors which will result in the solution having a small imaginary part, which may be ignored.

3.3. NOTE ON THE STRUCTURE OF THE EIGENSYSTEM AND THE SOLUTION OF THE HOMOGENEOUS EQUATION

It is shown in reference [11] that the eigenvalues of the general viscous equation (2) occur as complex conjugate pairs, say, $\lambda_j = \alpha_j + \mathrm{i}\beta_j$ and $\lambda_j^* = \alpha_j - \mathrm{i}\beta_j$ and that the corresponding

eigenvectors (modes) will also be complex conjugates. Hence, they have the pattern

$$\mathbf{x}_j = \mathbf{a}_j + \mathrm{i}\mathbf{b}_j \quad \text{and} \quad \mathbf{x}_j^* = \mathbf{a}_j - \mathrm{i}\mathbf{b}_j.$$

Consider the kth component of an eigenvector in polar form,

$$a_{jk} + \mathrm{i}b_{jk} = r_{jk}\mathrm{e}^{\mathrm{i}\theta_{jk}}, \quad k = 1 \ldots N,$$

where

$$r_{jk} = \sqrt{a_{jk}^2 + b_{jk}^2}, \quad \theta_{jk} = \arctan\left(\frac{b_{jk}}{a_{jk}}\right).$$

The component of the mode corresponding to the complex conjugate eigenvalue is

$$a_{jk} - \mathrm{i}b_{jk} = r_{jk}\mathrm{e}^{-\mathrm{i}\theta_{jk}}.$$

Thus, the kth components of

$$\mathrm{e}^{\lambda_j t}\mathbf{x}_j \quad \text{and} \quad \mathrm{e}^{\lambda_j^* t}\mathbf{x}_j^* \tag{20}$$

$$\text{are } \mathrm{e}^{(\alpha_j + \mathrm{i}\beta_j)t} r_{jk}\mathrm{e}^{\mathrm{i}\theta_{jk}} \quad \text{and} \quad \mathrm{e}^{(\alpha_j - \mathrm{i}\beta_j)t} r_{jk}\mathrm{e}^{-\mathrm{i}\theta_{jk}},$$

$$\text{or } \mathrm{e}^{\alpha_j t} r_{jk}\mathrm{e}^{\mathrm{i}(\beta_j t + \theta_{jk})} \quad \text{and} \quad \mathrm{e}^{\alpha_j} r_{jk}\mathrm{e}^{-\mathrm{i}(\beta_j t + \theta_{jk})}.$$

The pair of complex of functions given in equation (20) are solutions of the homogeneous form of equation (2)

$$\mathbf{M}\ddot{\mathbf{u}}(t) + \mathbf{C}\dot{\mathbf{u}}(t) + \mathbf{K}\mathbf{u}(t) = \mathbf{0}. \tag{21}$$

They, for $j = 1 \ldots N$, form a basis for the solution space and have the convenient form of separating the time and space variation. The space component can be viewed as a mode shape which in this case is complex. The physical meaning of complex mode shapes is discussed in references [13–15].

An alternative basis may be formed by recombining functions (20) into real functions. The real and imaginary parts of either of the pair may be used (alternatively the real and imaginary parts may be formed by a linear combination). It seems to be more meaningful when working in the time domain with real equations and real solutions to use these real basis functions,

$$\mathrm{e}^{\alpha_j t} r_{jk} \cos(\beta_j t + \theta_{jk}) \tag{22}$$

$$\text{and} \quad \mathrm{e}^{\alpha_j t} r_{jk} \sin(\beta_j t + \theta_{jk}), \quad j = 1 \ldots N. \tag{23}$$

The shape of mode j, $\mathbf{r}_j$, made from the components r_{jk} is modified through time by the decay term $\mathrm{e}^{\alpha_j t}$ and the sinusoidal term with the natural frequency β_j, rad/s, and a phase shift θ_{jk} for the component r_{jk}. An illustration is given later in Figure 5.

4. INFORMATION FROM THE MODEL

Here some predictions arising from using equation (2) with the approximating damping matrix $\mathbf{C}$ are examined. The need for such a matrix arose from work being carried out by

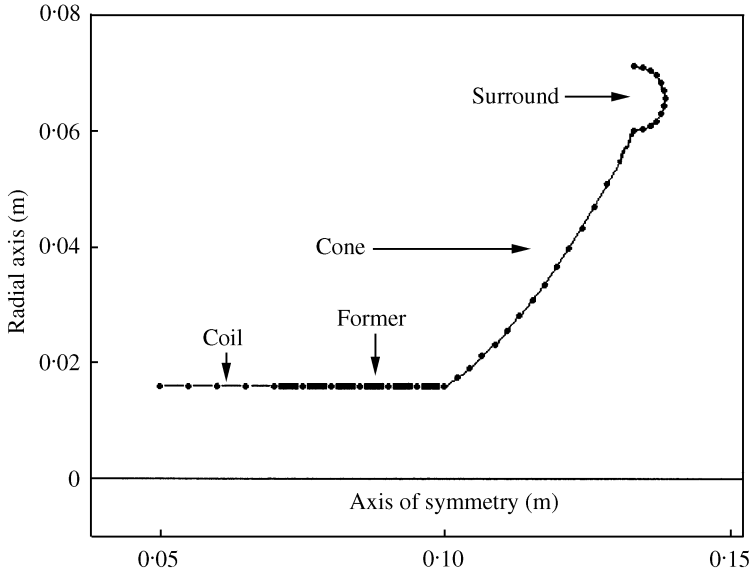

Figure 3. Finite element model of an axisymmetric loudspeaker diaphragm, coil and former.

a loudspeaker company on modelling the transient response of a diaphragm; the main concern in this paper is with the mathematics of the damping. A report on the acoustic justification and implications form a conference paper [16], to which an interested reader is referred. A slight overlap with that paper was necessary in order to verify the method against measured data, and Figures 10 and 11 are common.

4.1. THE STRUCTURE USED TO ILLUSTRATE THE METHOD

The structure used is a commercial loudspeaker cone shown in Figure 3. Values of the material properties used for the modelling were estimated and are given in Table 1.

4.2. VARIED DAMPING AND THE EIGENSYSTEM

Figure 4 shows the spread of natural frequencies and corresponding estimated modal loss factors using the material properties given in Table 1. The modal decay rates are available from the computation, but the corresponding modal loss factor is used for the y-axes in order to relate better with the loss factor assigned to the different materials of the structure. The modal loss factor is calculated using a relation (11) corresponding to a single-degree-of-freedom system,

$$\text{modal loss factor} = 2\,\frac{\text{decay rate}}{\text{modal frequency}}.$$

The modal loss factors shown in Figure 4 fall broadly into two groups, reflecting the surround value, 0·4, and that the cone, 0·07. Three modes at frequencies close to each other are chosen to illustrate different forms of behaviour, (a) at 3835 Hz, (b) at 3859 Hz and (c) at

TABLE 1

Material properties of the loudspeaker diaphragm, coil and former

Component	Material	E (MPa)	Density (kg/m^3)	Loss factor	Thickness (mm)
Coil		72 800	4800	0·008	0·550
Former	Kapton	5800	1000	0·003	0·245
Cone	Paper	3000	500	0·070	0·750
Surround	Rubber	3·5	1200	0·400	0·400

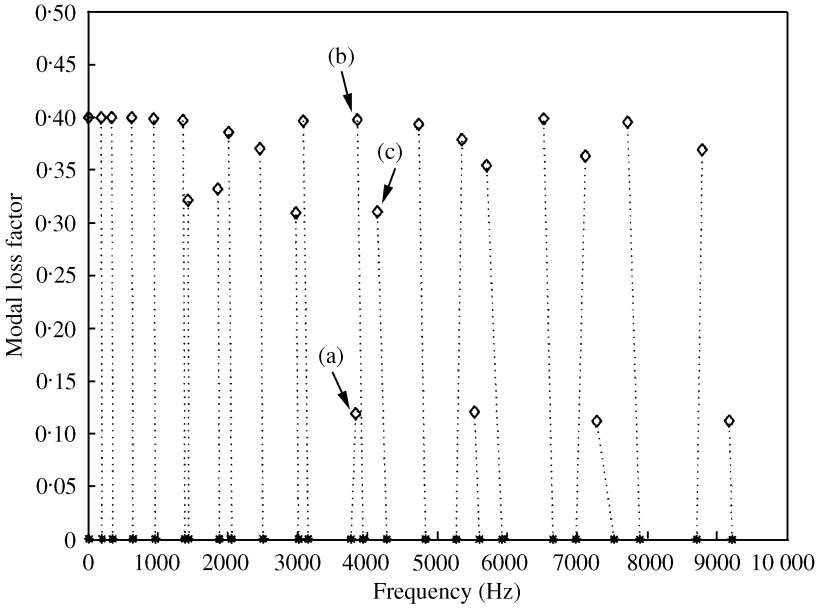

Figure 4. Estimated loss factor and frequencies of modes of the equivalent viscous damping method (◇) applied to the loudspeaker diaphragm with the material properties of Table 1. The undamped natural frequencies are shown by (∗). Three frequencies illustrate different types of behaviour, (a) low loss factor, 3835 Hz, (b) high loss factor, 3859 Hz, (c) middle value loss factor, 4145 Hz.

4145 Hz in Figure 4. The corresponding mode shapes, using the same lettering (a), (b) and (c) as for the frequencies, are shown in Figure 5. Two are at the extremes, near 0·4 and 0·07 and one has an intermediate loss value. The shapes displayed in Figure 5 are from equation (22) and are directly available from the computer code (nodes of the voice coil and former are included, also the node numbering starts at the coil and moves out to the surround). The low and high loss factors correspond to modes having motion mainly in the cone, (a), or surround, (b) respectively. The intermediate value, (c), has the motion more evenly distributed between the two components.

Notes on the damped modes and undamped natural frequencies of Figure 4

- The natural frequencies have been ordered and linked by dotted lines to the corresponding undamped natural frequencies; these show that mostly there is a decrease in frequency for the damped compared to undamped, which is as expected from the

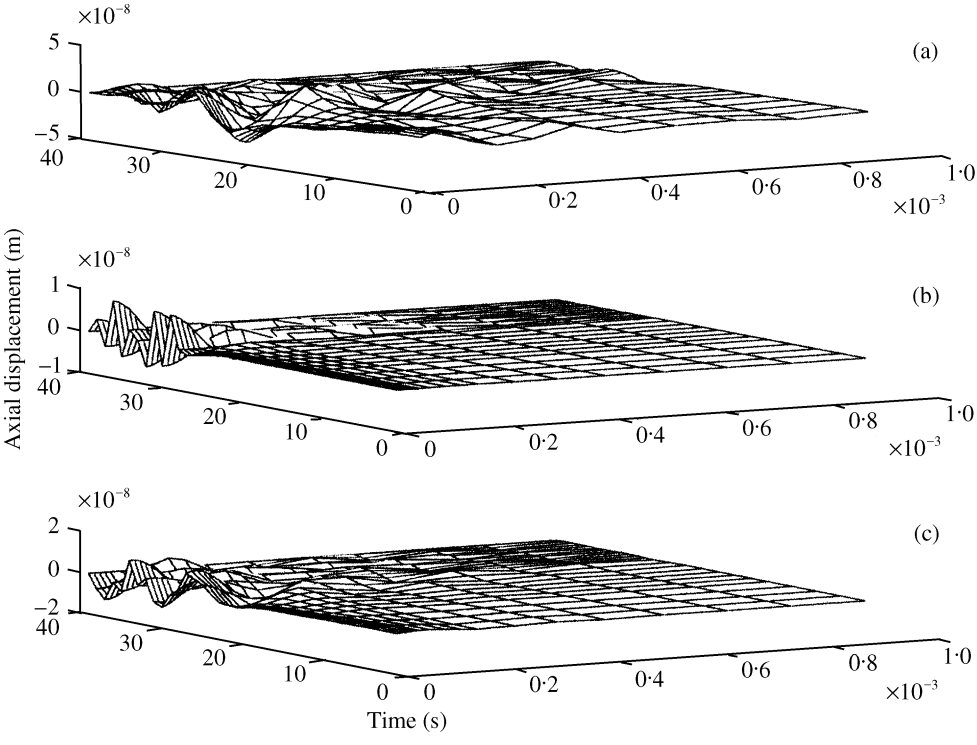

Figure 5. Three axial displacement modes (solutions of the homogeneous equation), corresponding to the (a) high, (b) middle value, and (c) low loss factors at the frequencies identified in Figure 4.

earlier one-degree-of-freedom analysis. However, in some cases there are very slight increases which are difficult to explain, though it is not thought to be significant.

- The significant material loss factors are $\eta = 0{\cdot}4$ for the surround and 0·07 for the cone. The estimated modal loss factors relate to where in the structure the motion of the mode dominates. If the motion is mainly in the surround then the loss factor is around 0·4, and if mainly in the cone, around 0·1. This is illustrated in Figure 5. This rather extreme form of behaviour results from the components being mismatched in terms of their mechanical impedance.
- Figure 5(a)–(c) also show that the loss factors relate directly with the decay rates.
- The modal loss factors lie between 0·1 and 0·4. No value goes above 0·4 although some are very close, closer than would be expected seeing that the motion is not located solely in one component. This may be partly explained by the method of computing the modal loss factor, see equation (11), the frequencies are under-estimated and the decay rates over-estimated which was previously noted when discussing Figure 2.

4.3. EVIDENCE ON REPRESENTING THE LOCATION OF DAMPING

The damping matrix **C** must be able to locate the damping in the material and the position at which it occurs, so that when a structure is excited the model should only dissipate energy in that area. It might seem that modal decomposition would make this difficult because the same loss factor applies for every point of a mode. However,

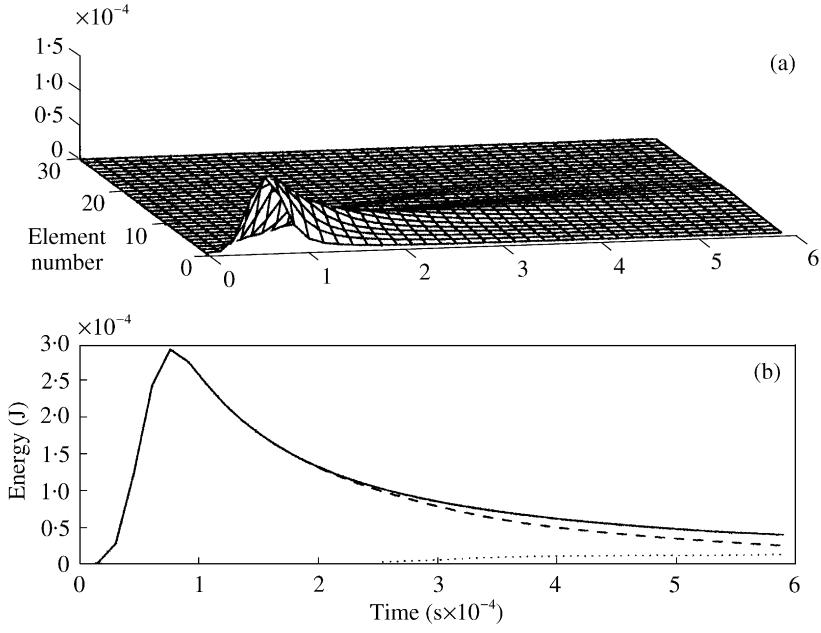

Figure 6. Energy movement through a disc with damping applied uniformly: energy is recorded for each element in (a), and in (b) summed for the inner half-disc (- - - -), outer half-disc (· · · ·), and total energy (——).

Figure 5 shows that motion of a mode can be mainly in one part of a structure, and Figures 6 and 7 show that the energy loss can similarly be localized.

Two numerical tests were carried out on the model of an aluminium disc with radius 60 mm, subjected to the impulsive force of a raised cosine, see section 4, with the frequency $\omega_0/2\pi = 10$ kHz, acting at the centre. The stiffness parameter and an unrealistically high loss factor of 0·4 were used in order to show clearly the different effects of damping and no damping in the inner half disc. The element energy is available in the computer code, as explained in section 3.2 and can be summed for regions or components of the structure. In Figure 6, the damping is uniform through the disc and the energy wave can be seen to move steadily outwards. The energy is input during the first 0·1 ms and the dissipation starts immediately. At around 0·2 ms the wave reaches the outer half disc, 30 mm $<$ radius $<$ 60 mm and energy can be seen to enter the region. The modelling is tested by removing the damping from the first half of the disc but otherwise keeping the material parameters the same. Figure 7 shows that the wave is then partially reflected by the mismatch at the half-way point, and most significantly there is only a very slight energy loss until this point is reached by the leading edge of the energy wave.

5. EVIDENCE OF THE QUALITY OF THE APPROXIMATION USING THE LOUDSPEAKER CONE

5.1. FREQUENCY DOMAIN COMPARISON

Both forms, the hysteretic and equivalent viscous approximation, may be applied directly in the frequency domain; a comparison was made over the range 500–10 kHz for the acceleration resulting from an impulse. Figure 8 shows the comparison at cross-sections at

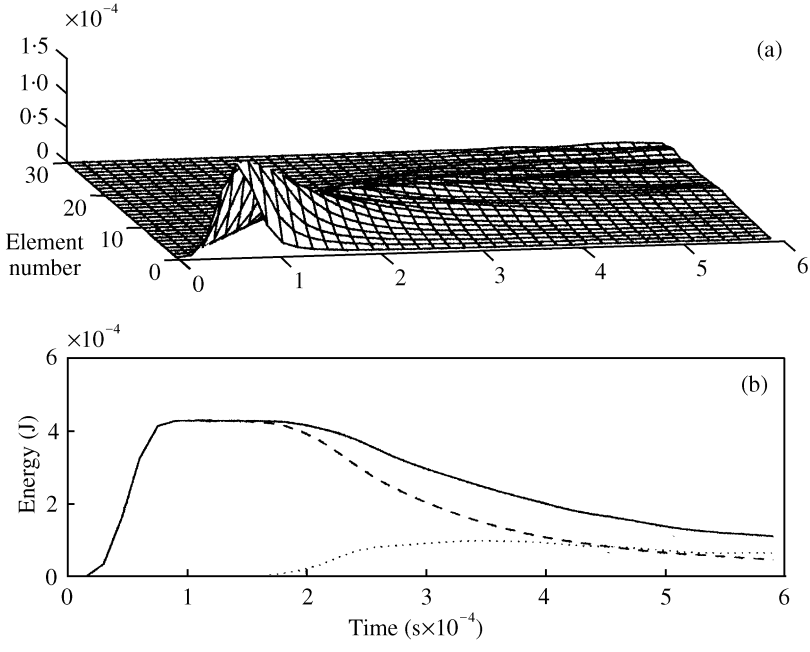

Figure 7. Energy movement through a disc with zero damping in the inner half-disc and damping in the outer part: energy is recorded for each element in (a), and in (b) summed for the inner half-disc (- - - -), outer half-disc (· · · ·), and total energy (——).

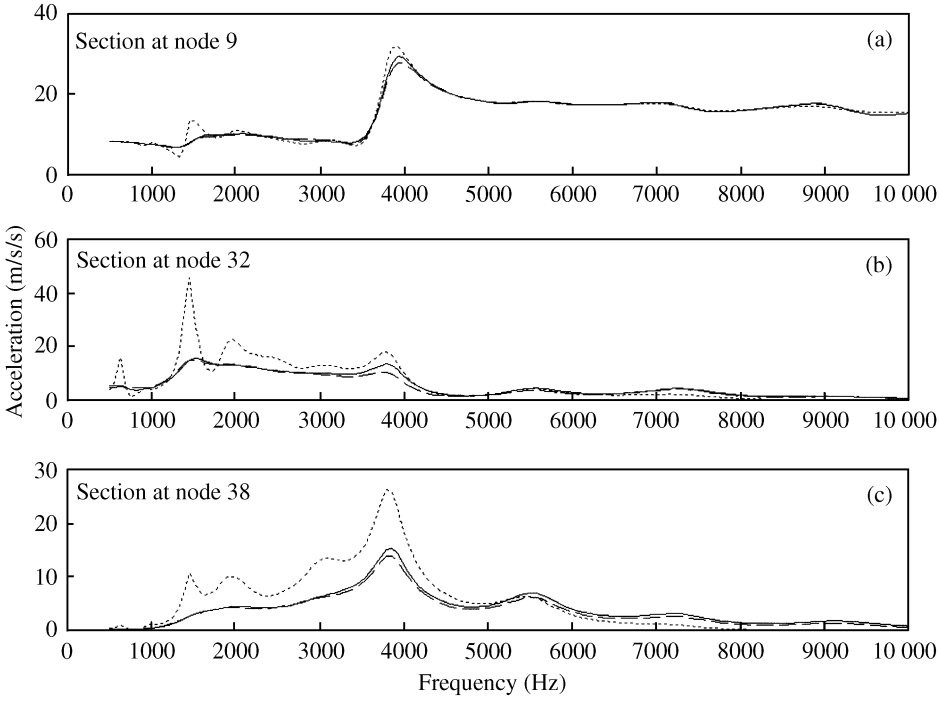

Figure 8. Detailed comparison of the normal component of acceleration in the frequency domain, between the hysteretic, equivalent viscous at the (a) coil/former join, (b) mid-cone, and (c) mid-surround positions. The —— and - - - - lines denote hysteretic values, and the equivalent viscous values respectively. The matched equivalent viscous values are given by · · · · lines.

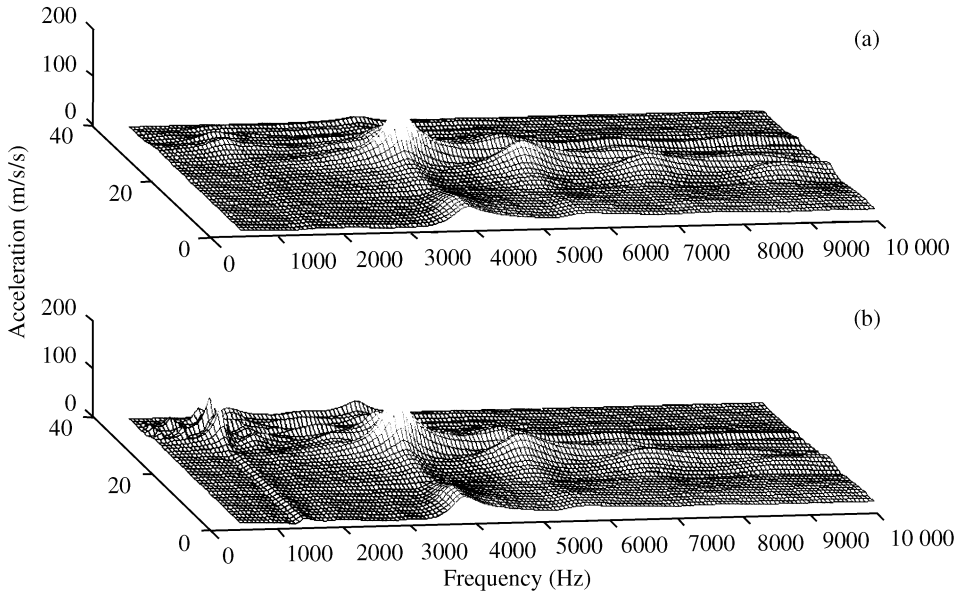

Figure 9. General comparison of the normal component of acceleration in the frequency domain between (a) hysteretic damping (the equivalent viscous model is very similar), and (b) the viscous damping model matched at a single frequency, 5250 Hz.

the former/cone join (a), mid-cone (b), and mid-surround (c) positions (see Figure 3). The detailed comparison shows little difference at the three chosen points; indeed, the full frequency plots for the hysteretic and equivalent viscous damping look to be the same and so both are not shown. In order to explore further a simpler viscous damping matrix was formed,

$$\mathbf{C} = \frac{1}{5250}\mathbf{H}.$$

This attempts to match hysteretic damping at the middle of the range rather than at all the natural frequencies. Values at the cross-sections is added in Figure 8, showing good agreement at the matched frequency with differences increasing away from it. A comparison for the whole structure is shown in Figure 9. The matching is good near the middle of the range and the single-matched damping under-estimates damping below the matching point and over-estimates above, as would be expected.

5.2. TIME DOMAIN COMPARISON

Since the time and frequency domains are equivalent, having verified the model in the frequency domain there is no formal need to consider further. However, the exact equivalence is based on a knowledge through infinite time and at all frequencies, which we do not have. In addition, there is some experimental evidence in the time domain from laser interferometry to compare against.

The hysteretic equation cannot be used directly in the time domain and has to be solved first in the frequency domain and then transformed by using the inverse fast Fourier

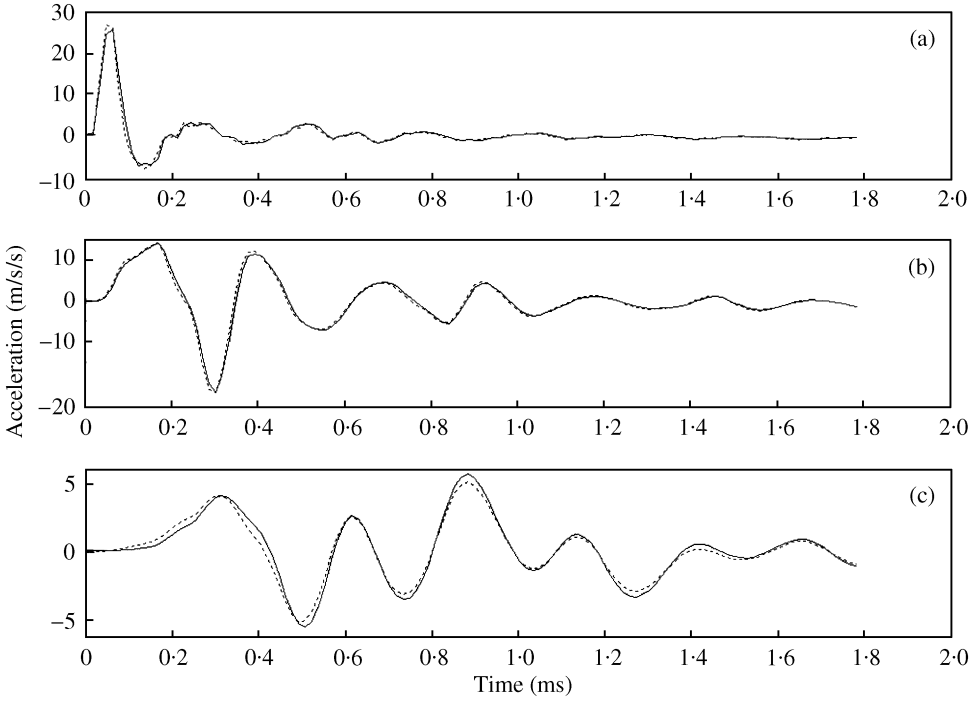

Figure 10. Detailed comparison in the time domain between the hysteretic (——), equivalent viscous (· · · ·), at the (a) former/cone join, (b) mid-cone, and (c) mid-surround positions.

transform. Equation (13) can be solved for $\omega > 0$ but in order to produce a real function for the time domain the rest of the frequency values have to be constructed. Suppose the solution for $\omega > 0$ is denoted by $\mathbf{U}_\delta(\omega)$. From the general transform theory

$$\mathbf{U}_\delta(-\omega) = [\mathbf{U}_\delta(\omega)]^*,$$

but equation (13) does not produce this. So $\mathbf{U}$ has to be constructed for negative ω.

$$\mathbf{U}_\delta(\omega) = \begin{cases} [\mathbf{M}\omega^2 + \mathrm{i}\mathbf{H} + \mathbf{K}]^{-1}\mathbf{p} & \text{if } \omega > 0, \\ [\mathbf{K}]^{-1}\mathbf{p} & \text{if } \omega = 0, \\ [\mathbf{M}\omega^2 - \mathrm{i}\mathbf{H} + \mathbf{K}]^{-1}\mathbf{p} & \text{if } \omega < 0, \end{cases}$$

where $\mathbf{p}$ is the position of the degrees of freedom at which the impulse is applied. Even after this necessary construction the signal will be acausal through the shape of the function $\mathbf{U}_\delta(\omega)$. Probably, though this is not serious, see reference [10]. Figures 10 and 11 are the response of the diaphragm to the same raised cosine pulse used to give the energy plots of section 4.3. The normal components of the accelerations predicted by the two methods are very similar and they are compared along the three sections used previously; this is shown in Figure 10. The greatest difference, although slight, is in the surround movement and is probably due to the higher level of damping.

The equivalent viscous damping method is compared with the laser measurements in Figure 11. The general features of the measured data are reproduced, sufficient to give

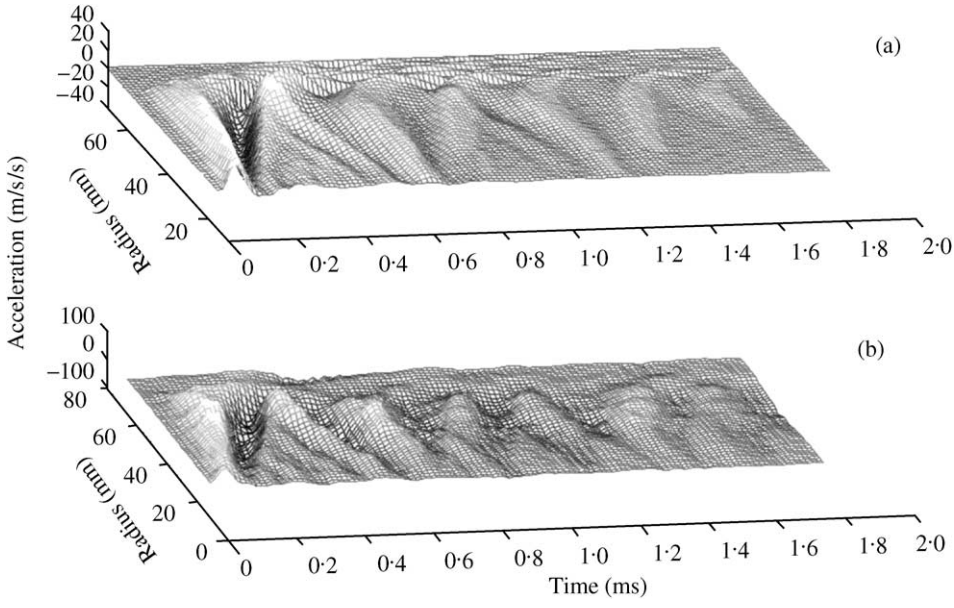

Figure 11. Comparison in the time domain of the normal component of acceleration between (a) the equivalent viscous damping model and (b) laser measurements.

confidence in the method. There are good reasons for the lack of detailed agreement; the theoretical model does not include the electrical circuit or the stabilizing device (the spider), and the material parameters are not precisely known.

6. CONCLUSIONS

The dynamic behaviour of a structure has been considered through a viscous damping model. Hysteretic damping is accepted as a standard and an equivalent viscous damping matrix **C** has been constructed, using the undamped eigensystem, which gives approximately the required frequency independence. The two forms gave good agreement when compared in the time and frequency domains in modelling a loudspeaker diaphragm. They were able to predict the main features shown in a response obtained through laser measurements. Using a circular aluminium plate model and considering energy dissipation the spatial information was shown to be well preserved in the equivalent model.

Using the developed matrix **C** the eigensystem was shown to contain information helpful in understanding motion of the structure. In an example with mis-matched materials solutions of the homogeneous equation (modes) were shown to have damping loss factors related to where they have their dominant motion.

ACKNOWLEDGMENTS

The author is grateful to the staff at the research centre of B&W Loudspeakers limited, Peter Fryer, Gary Geaves, and Jon Moore for initiating the work and giving their vital support. Also to the referees for their helpful suggestions which I have gratefully included, especially in more clearly defining the significance of the research.

REFERENCES

1. C. W. BERT 1973 *Journal of Sound and Vibration* **29**, 129–153. Material damping: an introductory review of mathematical measures and experimental techniques.
2. L. CREMER, M. HECKL and E. E. NGAR 1972 *Structure-borne Sound*, chapter 3. Berlin: Springer-Verlag.
3. S. H. CRANDALL 1970 *Journal of Sound and Vibration* **11**, 3–18. The role of damping in vibration theory.
4. D. R. BLAND 1960 *The Theory of Linear Viscoelasticity*. London: Pergamon Press.
5. Y. C. FUNG 1965 *Foundations of Solid Mechanics*, Englewood Cliffs, NJ: Prentice-Hall.
6. A. D. NASHIF, D. I. G. JONES and J. P. HENDERSON 1985 *Vibration Damping*. New York: Wiley-Interscience.
7. T. K. CAUGHEY 1960 *Journal Applied Mechanics* 269–271. Classical normal modes in damped linear systems.
8. M. E. MCINTYRE and J. WOODHOUSE 1978 *Acoustica* **39**, 209–224. The influence of geometry on linear damping.
9. J. WOODHOUSE 1998 *Journal of Sound and Vibration* **215**, 547–569. The role of damping in vibration theory.
10. W. H. PRESS, B. P. FLANNERY, S. A. TEUKOLSKY and W. T. VETTERLING 1992 *Numerical Recipes*. Cambridge: Cambridge University Press.
11. D. E. NEWLAND 1989 *Mechanical Vibration Analysis and Computation*. New York: Longman Scientific & Technical.
12. K. J. BARTHE and E. L. WILSON 1976 *Numerical Methods in Finite Element Analysis*. Englewood Cliffs, NJ: Prentice-Hall.
13. N. O. MYKLESTAD 1952 *Journal of Applied Mechanics* **19**, 284–287. The concept of complex damping.
14. I. IRIGUN and D. J. EWINS 1995 *Proceedings of the* 13*th International Modal Analysis Conference*, *Nashville*, *U.S.A*. Complex modes—origins and limits.
15. G. LALLEMENT and D. J. INMAN 1995 *Proceedings of the* 13*th International Modal Analysis Conference*, *Nashville*, *U.S.A*. A tutorial on complex eigenvalues.
16. G. P. GEAVES, J. MOORE, D. J. HENWOOD and P. A. FRYER 2001 *AES Convention Paper*, *Presented at the* 110*th Convention*, *Amsterdam*, *The Netherlands*. Verification of an approach for transient structural simulation of loudspeakers incorporating damping.